Title

Airborne observations of the tropospheric CO2 distribution and its controlling factors over the South Pacific Basin

Permalink

https://escholarship.org/uc/item/05j7f0w0

Journal

Journal of Geophysical Research, 104(D5)

ISSN

0148-0227

Authors

Vay, SA
Anderson, BE
Conway, TJ
et al.

Publication Date

1999-03-20

DOI

10.1029/98jd01420

Copyright Information

Peer reviewed

Airborne observations of the tropospheric CO_2 distribution and its controlling factors over the South Pacific Basin

S. A. Vay,[1] B. E. Anderson,[1] T. J. Conway,[2] G. W. Sachse,[3] J. E. Collins Jr.,[4] D. R. Blake,[5] and D. J. Westberg[6]

Abstract. Highly precise measurements of CO_2 mixing ratios were recorded aboard both the NASA DC-8 and P3-B aircraft during the Pacific Exploratory Mission-Tropics conducted in August–October 1996. Data were obtained at altitudes ranging from 0.1 to 12 km over a large portion of the South Pacific Basin representing the most geographically extensive CO_2 data set recorded in this region. These data along with CO_2 surface measurements from the National Oceanic and Atmospheric Administration/Climate Monitoring and Diagnostics Laboratory (NOAA/CMDL) and the National Institute of Water and Atmospheric Research (NIWA) were examined to establish vertical and meridional gradients. The CO_2 spatial distribution in the southern hemisphere appeared to be largely determined by interhemispheric transport as air masses with depleted CO_2 levels characteristic of northern hemispheric air were frequently observed south of the Intertropical Convergence Zone. However, regional processes also played a role in modulating background concentrations. Comparisons of CO_2 with other trace gases indicated that CO_2 values were influenced by continental sources. Large scale plumes from biomass burning activities produced enhanced CO_2 mixing ratios within the lower to midtroposphere over portions of the remote Pacific. An apparent CO_2 source was observed in the NOAA/ CMDL surface data between 15°N and 15°S and in the lower altitude flight data between 8°N and 8.5°S with a zone of intensity from 6.5°N to 1°S. Inferred from these data is the presence of a Southern Ocean sink from south of 15°S having two distinct zones seasonally out of phase with one another.

1. Introduction

"Fixed air," or carbon dioxide (CO_2), was first noted in 1754 by physician Joseph Black [*Jaffe*, 1942], and the earliest records of atmospheric CO_2 measurements are described in the nineteenth century literature [*Callendar*, 1958]. However, prior to the late 1950s, the atmospheric concentration of CO_2 was thought to exhibit significant variability until precise and accurate measurements utilizing infrared absorption and manometric techniques were instituted by C. D. Keeling. As an offshoot of this initial work, an extensive global surface network currently exists for measurements of CO_2 and its isotopes yet, despite these efforts, much remains uncertain in terms of the global carbon budget. Contributing to these uncertainties are unprecedented human disturbances of the atmosphere predominantly in the form of fossil fuel combustion and, to a lesser degree, land use changes. In 1995, for example, the global annual CO_2 emission from the burning of fossil fuels, including gas flaring, and hydraulic cement production was estimated at 6.4 GtC (1 GtC = 1 billion (10^9) tons of carbon) compared with 1.6 GtC in 1950 [*Marland et al.*, 1997].

To date, there is no clear consensus as to whether human activities have altered climate. Recent work by *Santer et al.* [1996] has shown an increasing trend in the similarity between observed and model-predicted spatial patterns of temperature change in the free atmosphere from 1963 to 1987 using a model incorporating various combinations of changes in CO_2, anthropogenic sulphate aerosol and stratospheric ozone concentrations. Their results suggest that this trend is partially attributable to human activities. Clouding the picture is the increasing difficulty in separating out changes that are part of short or long term natural trends from those which are anthropogenically induced. What is quite evident however, is that CO_2 has increased in concentration since the mid 1800's from a preindustrial value of ~280 ppm to a current one of ~360 ppm [*Intergovernmental Panel on Climate Change (IPCC)*, 1990] owing primarily to the burning of fossil fuels, 90% of which occurs in the northern hemisphere [*Marland and Boden*, 1991].

Previously, CO_2 emissions have been closely linked to economic growth, industrialization, and overall energy consumption [*IPCC*, 1992], therefore these levels may continue to rise as developing countries seek to improve standards of living and the world's population enlarges. However, *Keeling et al.* [1995] points out that environmental factors appear to have imposed larger changes on the rate of rise of atmospheric CO_2 since 1980 than did changes in fossil fuel combustion rates. Many multidisciplinary studies have been undertaken to assess these factors such as the effects of a CO_2-enriched atmosphere on various biogeochemical cycles. Recent results from these studies suggest that potential shifts in ecosystem physiology could inevitably be the important controllers of carbon fluxes.

In an effort to expand our current level of understanding regarding this trace gas, airborne measurements of tropospheric

[1]Atmospheric Sciences Division, NASA Langley Research Center, Hampton, Virginia.

[2]Climate Monitoring and Diagnostics Laboratory, National Oceanic and Atmospheric Administration, Boulder, Colorado.

[3]Aerospace Electronic Systems Division, NASA Langley Research Center, Hampton, Virginia.

[4]Science and Technology Corporation, Hampton, Virginia.

[5]Department of Chemistry, University of California, Irvine.

[6]Science Applications International Corporation, Hampton, Virginia.

CO_2 were undertaken in the South Pacific Basin; a region relatively uncharted above the planetary boundary layer. Prior aircraft measurements in this portion of the southern hemisphere were focused over the Australian-New Zealand region and south to Antarctica [*Pearman and Beardsmore*, 1984], Japan to Australia [*Nakazawa et al.*, 1991; *Matsueda and Inoue*, 1996], and the United States to Tahiti [*Anderson et al.*, 1996]. The following text therefore describes the first extensive airborne CO_2 data set encompassing the breadth of the basin. These data provide valuable information on the spatial distributions of CO_2 which can be used to develop, test, and enhance the predictive abilities of 3-D global CO_2 models and foster a better understanding of the global carbon cycle.

2. Experiment

The Pacific Exploratory Mission-Tropics (PEM-T) was designed as an intensive airborne campaign over the South Pacific Basin with the primary objectives of providing baseline data on the chemical species important in controlling the oxidizing power of the troposphere and the factors governing their concentrations. Since the atmosphere in this remote geographic region is relatively unexplored and possibly the most pristine globally, a background level assessment of these chemical species was considered crucial before anthropogenic inputs increase further from expanding economies and population growth.

PEM-T coincided with the austral late winter/early spring, when biomass burning reaches its seasonal maximum (August–October) in the southern tropics [*Kirchhoff et al.*, 1996]. It encompassed a total of 34 science flights conducted by two different research aircraft: the P3-B based out of NASA Wallops Flight Facility located in Virginia and the NASA DC-8 stationed at Ames Research Center, Moffett Field, California. The Lockheed Orion P3-B is capable of speeds of 140–170 ms^{-1}, with an operating altitude range of 0.1 km to 8.6 km, and a maximum flight duration of 12 hours. The McDonnell Douglas DC-8 has a nominal airspeed of 225 ms^{-1} at cruise altitude, a flight duration

of 12 hours, and an altitude range of 0.3 km to 12.8 km. Actual flight tracks for the DC-8 during the mission are presented in Figure 1 whereas those for the P3-B are shown in Figure 2. Flight patterns typically consisted of constant altitude legs, ramps, spirals, and additionally in the case of the P3-B, Lagrangian circles. Bases of operation were located at Hawaii (Oahu), Christmas Island, Tahiti, Fiji, New Zealand (Christchurch), Easter Island, and Ecuador (Guayaquil) and provided excellent opportunities for good aerial spatial coverage of the basin longitudinally from 170°E to 80°W as well as meridionally from 20°N to 72°S. A listing of the science flights used in this subsequent analysis can be found in Table 1 which includes both temporal and spatial information. For a more detailed account of the mission see *Hoell et al.* [this issue].

Both aircraft were equipped with a suite of instrumentation capable of measuring a number of species including CO_2, CO, CH_4, NO_x, O_3, $H_2O_{(g)}$, sulfur species, peroxides, and aerosols. Additional species measured on only one of the two aircraft were OH, PAN, as well as O_3 and aerosols by a nadir and zenith-looking remote sensor. Nonmethane hydrocarbons (NMHC) and halocarbon concentrations were determined from pressurized whole air samples collected in stainless steel canisters on both aircraft that were shipped after each flight to the University of California-Irvine laboratory for analysis [*D. Blake et al.*, 1996; *N. Blake et al.*, 1996]. The DC-8 and P3-B CO_2 data were obtained with LI-COR model LI-6252 differential, non-dispersive infrared gas analyzers. CO_2 measurements with these instruments are based on the difference in absorption of infrared radiation between the reference and sample gases that flow continuously through identical optical absorption cells. For PEM-T, the instruments were operated at constant pressures and mass flows of 250 torr and 400 $cm^3 min^{-1}$, respectively. Each LI-COR unit was mounted on a vibrationally isolated optical table with a two channel, mid-IR tunable diode laser-based differential absorption instrument designed for measurements of CO and CH_4 and referred to as Differential Absorption CO Measurement (DACOM). Both instruments shared a common inlet, associated

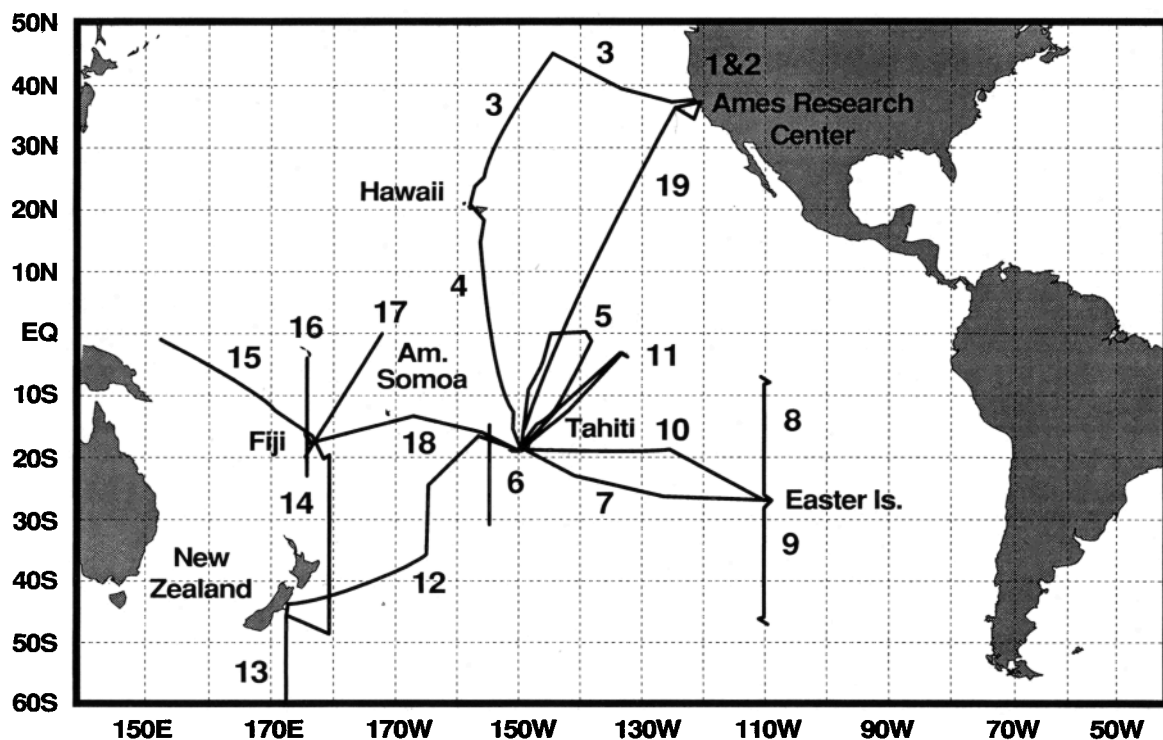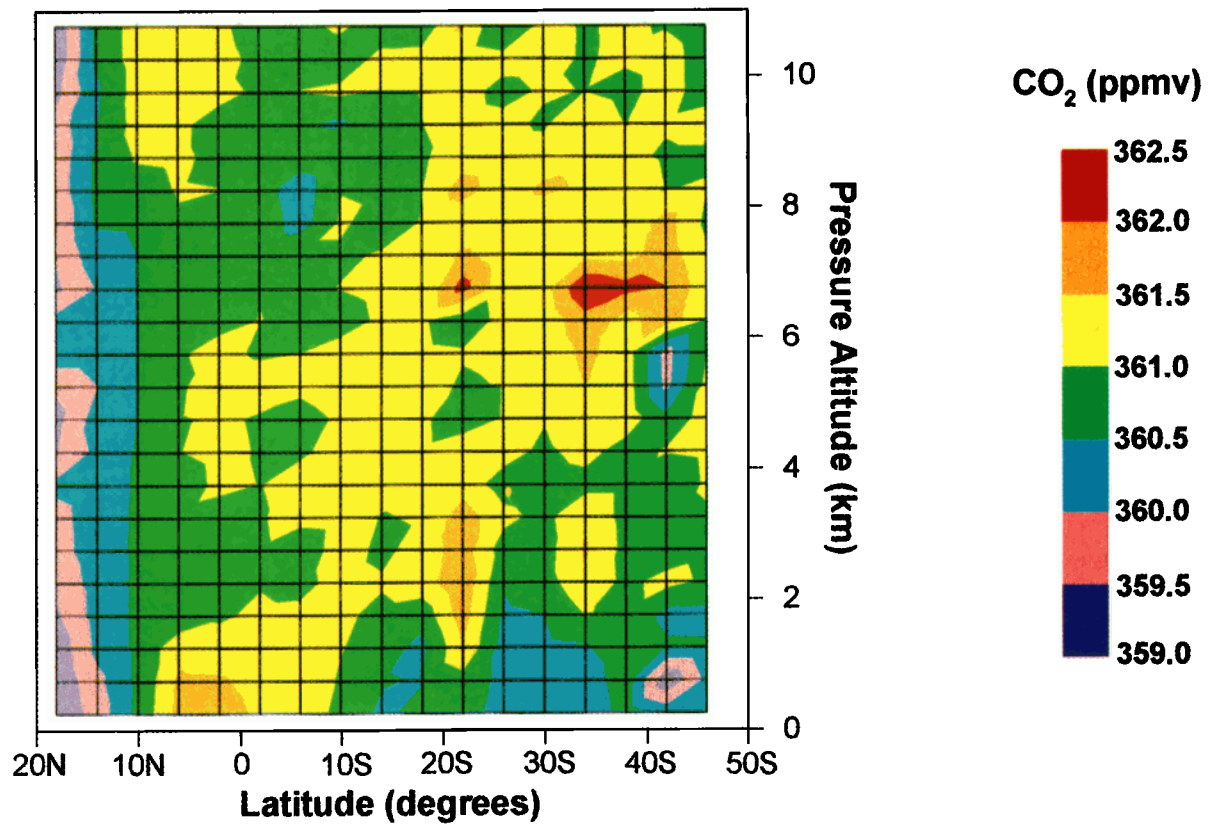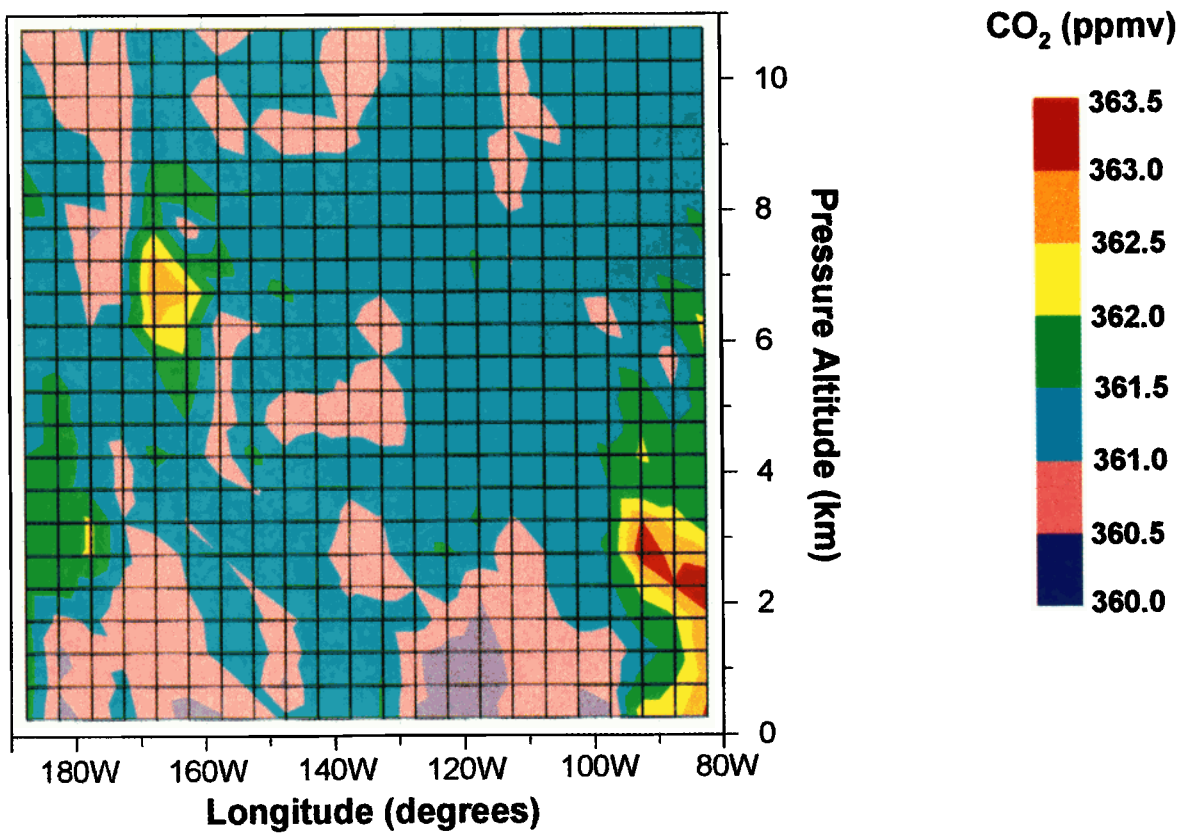

Figure 1. PEM-T DC-8 flight tracks.

Plate 1. PEM-T zonal mean concentration of CO_2 between 107.5°W and 152.5°E longitude as a function of latitude and altitude.

Plate 2. PEM-T meridional mean concentrations of CO_2 between the equator and 35°S as a function of longitude and altitude.
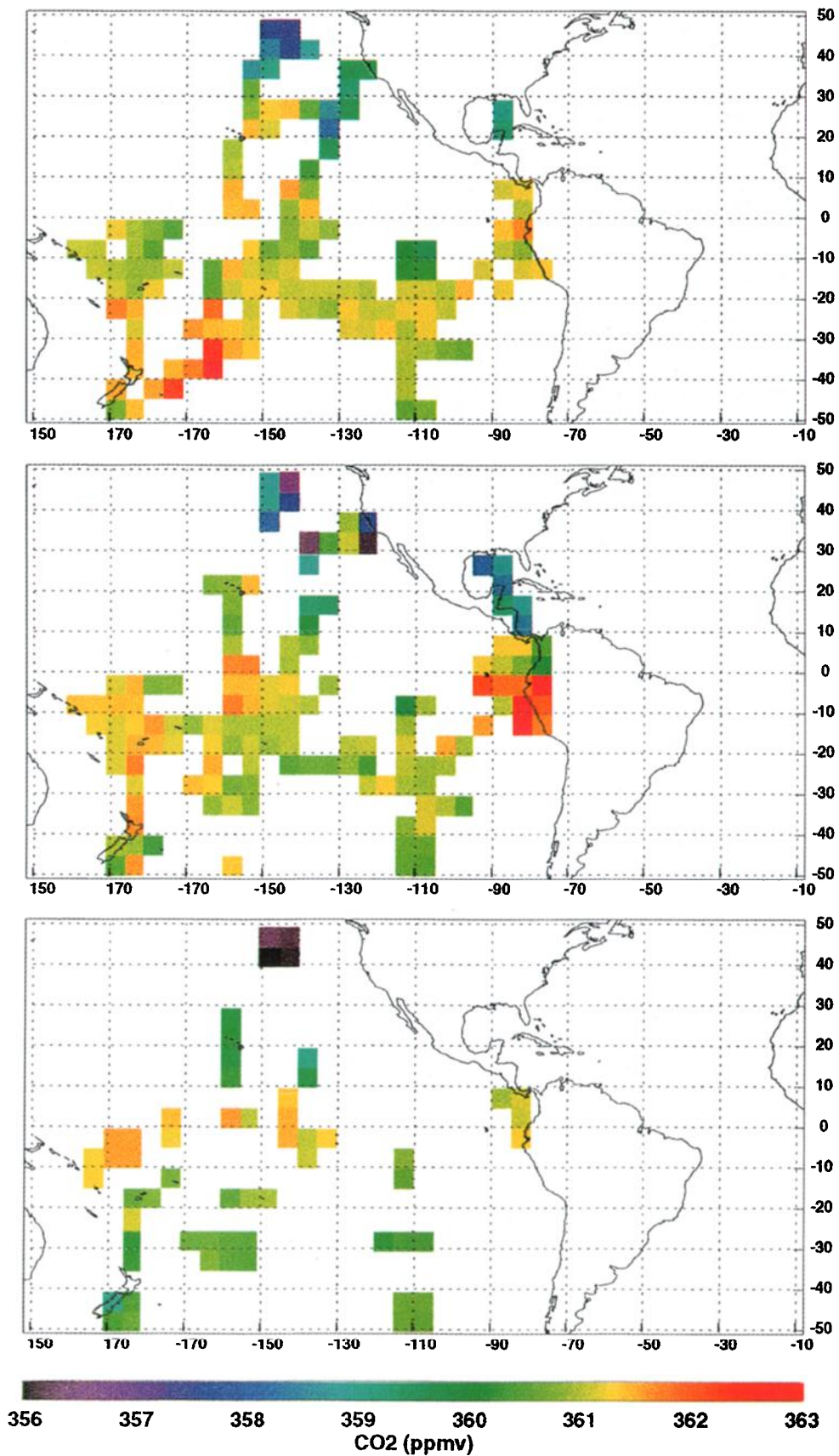
Plate 3. Regional distribution of CO_2 during PEM-T for (a) 0–2 km, (b) >2–6 km, and (c) >6–12 km altitude ranges. Data were grouped into 5° × 5° bins and then averaged.

plumbing, and data acquisition system. Ambient air was drawn in via a Rosemont probe, dried, compressed and then apportioned to the LI-COR and DACOM. Nafion gas dryers (Perma Pure, Inc.) were used to reduce the sample dew point to $\leq -40°C$ thus eliminating the need for applying water vapor corrections to the CO_2 data while the compressor was required for high-altitude sampling. Laboratory studies demonstrated that these additional flow components do not affect the incoming analytes.

Baseline drift was checked at 10 min intervals by introducing, upstream of the dryers, primary reference gas obtained from the NOAA Climate Monitoring and Diagnostics Laboratory (CMDL). This reference gas (two cylinders were used on each aircraft during the mission) was actually a compressed ambient air sample from Niwot Ridge, Colorado, having a CO_2 concentration established relative to primary standards traceable to the World Meteorological Organization (WMO) Central CO_2 Laboratory at the Scripps Institution of Oceanography [*Thoning et al.*, 1989]. The calibration transfer accuracy from the WMO standards to the NOAA standards was estimated at ±0.2 ppmv [*Conway and Steele*, 1989]. At approximately 2 hour intervals, the instrument sensitivity or "span" was verified by flowing a second standard (span gas) through the LI-COR sample cell having a CO_2 mixing ratio 10–15 ppmv higher than the reference gas. This span gas was a synthetic air mixture purchased from Scott Marrin (Riverside, California) and shipped to NOAA/CMDL for CO_2 analysis using the same methods that established the reference gas concentration. Checks of the instrument zero were performed at least three times per flight by introducing reference gas simultaneously into both absorption cells of the LI-COR. An additional check of the CO_2 calibration was provided when a synthetic air mixture devoid of CO and CH_4 was run through the system at least twice per flight in order to establish a zero level for the DACOM system. Post-mission analysis of the standards by NOAA/CMDL showed no measurable change from pre-mission CO_2 values. Data were recorded at 1 Hz and archived at 5 s intervals. For the PEM-T CO_2 5 s data, we have determined a precision of ±0.05 ppmv (1σ) with an accuracy relative to WMO standards of ±0.3 ppmv. Stratospherically influenced data, identified by $O_3 > 100$ ppbv with concomitant decreases in the tracers CO and CH_4, were removed. A more detailed description of the CO_2 and DACOM instruments and their operation is given by *Anderson et al.* [1996], and *Sachse et al.* [1988], respectively.

Surface data from the NOAA/CMDL network will be presented therefore a brief summary of their procedures will be given here. See *Conway et al.* [1988, 1994] and *Komhyr et al.* [1983] for more detail. For the land-based sites, individual flask samples are collected in pairs at weekly intervals using 2.5-L glass flasks equipped with two Teflon O-ring stopcocks by means of a portable pumping unit. Flask samples from container ships participating in the network program are collected in evacuated 3-L flasks approximately one sample pair every 1.5 weeks per 5° latitude. Flasks are shipped to Boulder, Colorado, for subsequent analysis utilizing a Siemens Ultramat 3 nondispersive infrared analyzer. CO_2 concentrations are established relative to primary standards maintained by the WMO Central CO_2 Laboratory at the Scripps Institution of Oceanography. If a sample pair has a difference >0.5 ppm, both members are automatically rejected. Members can also be excluded if the CO_2 concentration is not representative of background air (>3σ from fitted curve), or some problem arose during sampling, shipping, or analysis. The NOAA/CMDL CO_2 values presented in this study are interpolations obtained from curves fitted to the data using routines described by *Thoning et al.* [1989].

3. Results and Discussion

3.1. Spatial Distributions: The Big Picture

A snapshot of the zonal mean CO_2 concentration as a function of latitude and altitude is depicted in Plate 1. This plot was prepared from a 4° latitude by 0.25 km altitude grid of average values over the geographic range of 18°N to 46°S and 107.5°W to 152.5°E and therefore excludes the P3-B flights based out of Guayaquil, South America. The extensive aerial coverage of the basin resulted in the estimation of only 11% of the grid points using an inverse-distance weighting algorithm (SigmaPlot, Jandel Scientific). This plot illustrates several important features: (1) During PEM-T, the highest CO_2 mixing ratios were observed in the southern hemisphere (SH). (2) Lower northern hemispheric (NH) CO_2 levels are propagating southward at higher altitudes. (3) A CO_2 source in the equatorial region exists at the lower levels. (4) Lower CO_2 mixing ratios underlie the midtroposphere in the SH.

Longitudinal variations have typically been overlooked since atmospheric mixing often occurs much faster in the east-west than the north-south direction and due to the paucity of longitudinal data. Zonal variations are expected due to atmospheric dynamics and the nonuniform distribution of CO_2 sources and sinks [*Nakazawa et al.*, 1991]. Plate 2 is a 5° longitude by 0.25 km altitude grid of average values over 0° to 35°S and 82.5°W to 172.5°E. The latitude band for this plot was chosen in order to minimize the amount of interpolation required for missing grid values which totaled 15% of all grid points. Apparent in this plate is (1) The influence of land masses bordering the basin on CO_2 concentrations, (2) Relative zonal homogenity of CO_2 mixing ratios in the central basin, and (3) NH air depleted in CO_2 at higher altitudes gradually diffusing into or mixing with air in the lower levels.

A different perspective on these data is given in Plates 3a–3c where 5° latitude by 5° longitudinal bins containing averaged CO_2 values have been superimposed on geographic maps of the PEM-T sampling region. Here, the data are presented in three different altitude regimes: the planetary boundary layer (PBL) (0–2 km), the lower free troposphere (2–6 km), and the middle to upper free troposphere (6–12 km). Representations of this form give a more detailed spatial accounting of the CO2 distributions on an almost flight by flight basis when compared with the flight track maps shown in Figures 1 and 2 and enable one to pinpoint the locations of potential CO_2 source/sink zones that were illustrated in Plates 1 and 2. We find that in the PBL, the highest CO_2 concentrations appear in the equatorial region with no significant surface sources at the more southerly latitudes. The lower free tropospheric levels are clearly dominated by the elevated concentrations found over and off the coast of western South America and to a lesser extent New Zealand, Fiji, and the equator. At the 6 to 12 km level, the highest CO_2 mixing ratios were encountered enroute from Tahiti to New Zealand. Sites of interhemispheric transport are indicated north of Easter Island and Fiji, and northeast of Tahiti. In all three altitude bins, the lowest CO_2 mixing ratios are in the NH. These features are further addressed in the ensuing discussion.

3.2. Vertical and Meridional Gradients

Data from the NOAA/CMDL network were provided for incorporation into this study enabling vertical profiles of the CO_2 data to be constructed from the surface to 12 km over a portion of the sampling region where good overlap between surface and air-
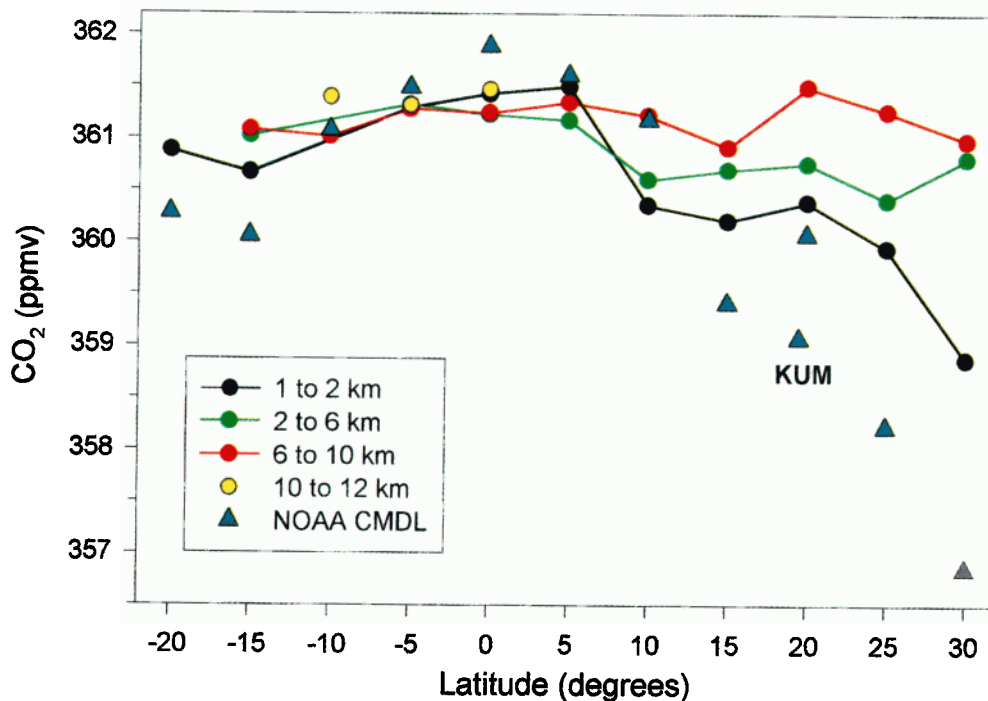
Plate 4. Vertical and meridional gradients for the central Pacific region from August 18 to 31, 1996.
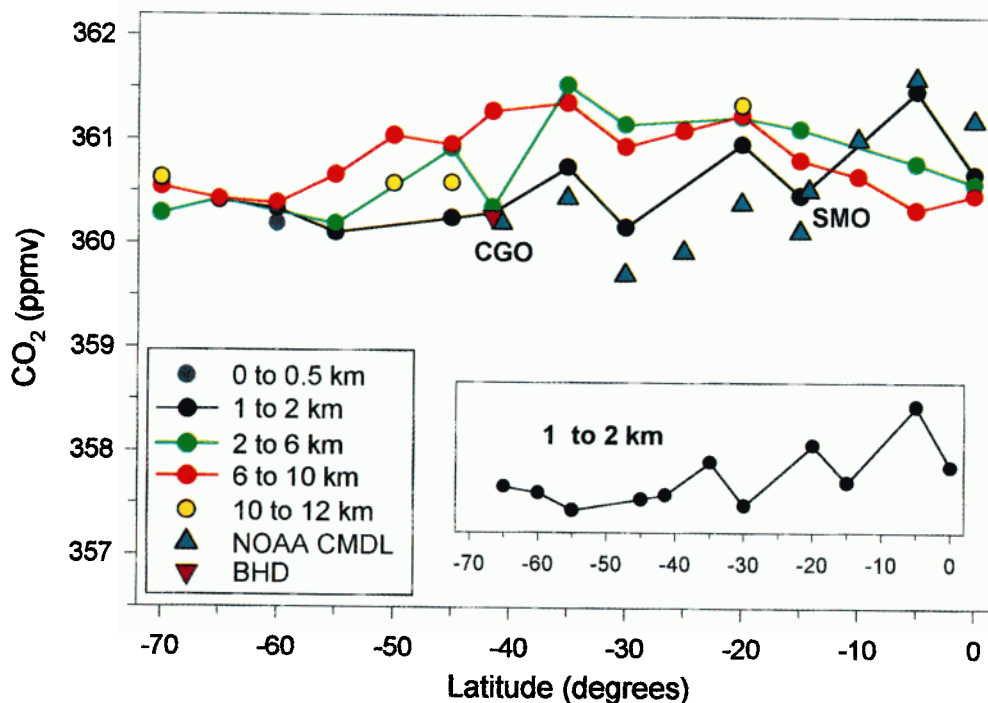

Plate 5. Vertical and meridional gradients for the western South Pacific Basin from September 22 to October 1, 1996.

craft data existed. Surface data presented, unless indicated otherwise, are from NOAA/CMDL shipboard flask samples that are collected at approximately 5° latitude intervals on regular cruises of the California Star (OPC) and the Brisbane Star (OPB) in the Pacific Ocean between the west coast of the United States and New Zealand. Because of the low sampling frequency in each latitude bin, the OPC and OPB data are combined to form the Pacific Ocean Cruises (POC) that are listed in Table 2 along with other site information. Surface data from the NOAA/ CMDL

Christmas Island site were unavailable for inclusion in this analysis due to logistical problems. Figure 3 depicts actual ship tracks and surface site locations. The solid lines connecting latitude bins in Plates 4 and 5, which illustrate the surface and flight data, are for purposes of clarity to the reader only. Statistics for these plots can be found in Tables 3 and 4.

In order to maximize the latitudinal coverage, it was necessary to use data from the beginning and ending periods of the mission which are separated temporally by approximately 4–6 weeks.
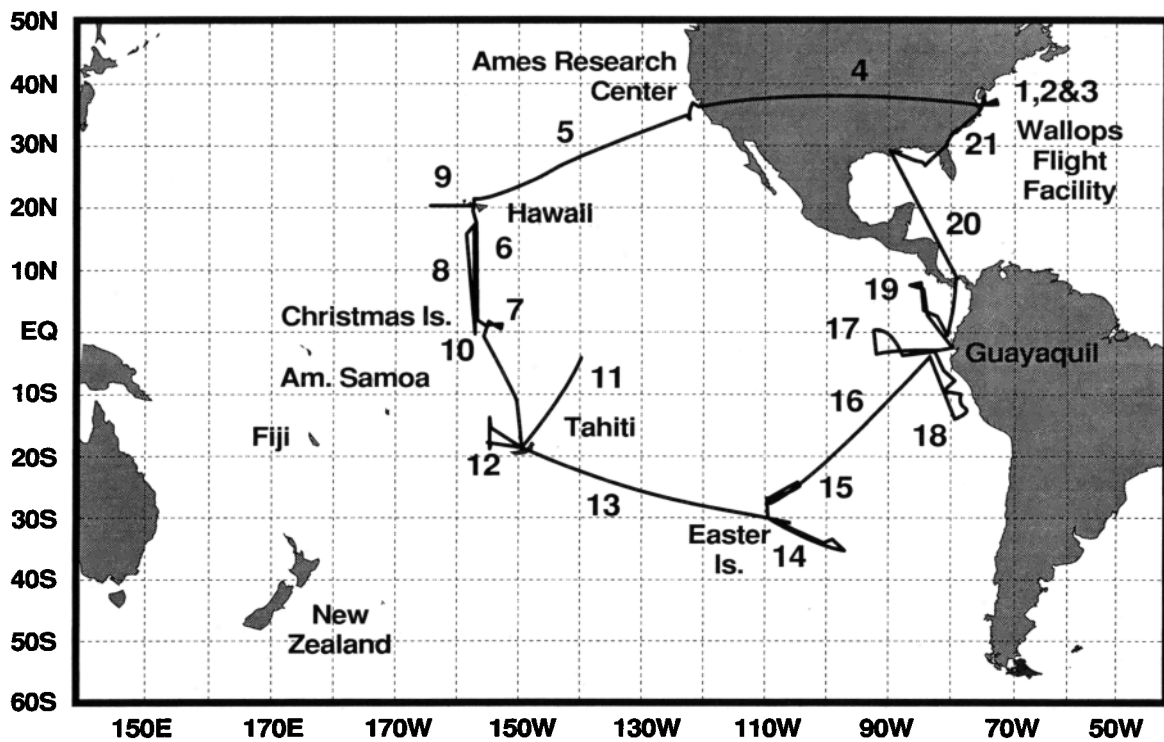
Figure 2. PEM-T P3-B flight tracks.

Table 1. Flights Used in CO_2 Data Analysis

Flight Number	Flight Date, UTC	Takeoff Site	Landing Site	Latitude Range	Longitude Range
DC-8					
3	Aug. 30, 1996	Ames	Hawaii	45°10′N–21°14′N	128°06′W–157°44′W
4	Aug. 31, 1996	Hawaii	Tahiti	20°55′N–17°43′S	157°15′W–149°40′W
5	Sept. 3, 1996	Tahiti	Tahiti	17°40′S–00°00′	149°52′W–138°31′W
6	Sept. 5, 1996	Tahiti	Tahiti	15°17′S–30°34′S	149°33′W–155°24′W
7	Sept. 7, 1996	Tahiti	Easter	17°53′S–27°19′S	148°21′W–108°52′W
8	Sept. 10, 1996	Easter	Easter	27°11′S–07°15′S	109°14′W–110°29′W
9	Sept. 11, 1996	Easter	Easter	27°01′S–47°08′S	109°12′W–111°02′W
10	Sept. 14, 1996	Easter	Tahiti	27°00′S–17°47′S	109°54′W–149°23′W
11	Sept. 16, 1996	Tahiti	Tahiti	17°26′S–03°35′S	149°30′W–133°09′W
12	Sept. 18, 1996	Tahiti	NZ	16°44′S–44°23′S	149°38′W–172°29′E
13	Sept. 21, 1996	NZ	NZ	43°32′S–72°33′S	172°57′E–171°27′E
14	Sept. 24, 1996	NZ	Fiji	48°16′S–17°51′S	172°14′E–179°15′E
15	Sept. 27, 1996	Fiji	Fiji	17°37′S–00°35′S	177°22′E–152°37′E
16	Sept. 29, 1996	Fiji	Fiji	22°14′S–03°30′S	177°18′E–174°44′E
17	Oct. 1, 1996	Fiji	Fiji	19°41′S–00°03′N	175°43′E–172°54′W
18	Oct. 3, 1996	Fiji	Tahiti	17°43′S–13°23′S	177°25′E–149°34′W
19	Oct. 5, 1996	Tahiti	Ames	17°59′S–37°20′N	149°17′W–122°09′W
P3-B					
5	Aug. 18, 1996	Ames	Hawaii	37°26′N–21°20′N	122°03′W–157°58′W
6	Aug. 21, 1996	Hawaii	Christmas	21°18′N–1°59′N	156°13′W–158°04′W
7	Aug. 24, 1996	Christmas	Christmas	02°11′N–00°51′N	157°25′W–153°20′W
8	Aug. 26, 1996	Christmas	Hawaii	01°40′N–21°24′N	158°46′W–157°08′W
9	Aug. 30, 1996	Hawaii	Hawaii	21°03′N–21°28′N	164°31′W–157°56′W
10	Aug. 31, 1996	Hawaii	Tahiti	20°54′N–17°43′S	158°19′W–149°37′W
11	Sept. 3, 1996	Tahiti	Tahiti	17°34′S–02°49′S	149°39′W–140°24′W
12	Sept. 5, 1996	Tahiti	Tahiti	17°51′S–13°10′S	155°39′W–149v35′W
13	Sept. 7, 1996	Tahiti	Easter	27°09′S–17°22′S	149°29′W–109°26′W
14	Sept. 10, 1996	Easter	Easter	34°50′S–25°53′S	110°08′W–97°23′W
15	Sept. 11, 1996	Easter	Easter	29°39′S–22°26′S	110v14′W–103°32′W
16	Sept. 14, 1996	Easter	Ecuador	27°06′S–01°13′S	109°14′W–79°47′W
17	Sept. 18, 1996	Ecuador	Ecuador	03v01′S–01°11′N	93°14′W–79°45′W
18	Sept. 22, 1996	Ecuador	Ecuador	13°38′S–02°01′S	83°27′W–78°01′W
19	Sept. 23, 1996	Ecuador	Ecuador	02°12′S–08°29′N	79°48′W–86°39′W

Ranges comprise geographic areas where CO_2 data are available.

Table 2. NOAA and NIWA Site Information for Selected Stations

Site Code	Site	Latitude	Longitude	Site Elevation, m
BHD	Baring Head, New Zealand	41°29'S	174°52'E	80
CGO	Cape Grim, Tasmania	40°41'S	144°41'E	94
SMO	American Somoa	14°15'S	170°34'W	30
KUM	Cape Kumukahi, Hawaii	19°31'N	154°49'W	3
POCN30	Pacific Ocean	30°00'N	150°11'W–122°17'W	
POCN25	Pacific Ocean	25°00'N	154°37'W–127°00'W	
POCN20	Pacific Ocean	20°00'N	158°25'W–131°38'W	
POCN15	Pacific Ocean	15°00'N	161°14'W–136°01'W	
POCN10	Pacific Ocean	10°00'N	163°50'W–140°23'W	
POCN05	Pacific Ocean	05°00'N	166°36'W–144°37'W	
POC000	Pacific Ocean	00°00'	169°16'W–148°52'W	
POCS05	Pacific Ocean	05°00'S	171°57'W–153°05'W	
POCS10	Pacific Ocean	10v00'S	174°40'W–157°20'W	
POCS15	Pacific Ocean	15°00'S	178°03'W–163°00'W	
POCS20	Pacific Ocean	20°00'S	173°28'W–177°44'E	
POCS25	Pacific Ocean	25°00'S	177°00'W–176°56'E	
POCS30	Pacific Ocean	30°00'S	179°30'E–176°04'E	
POCS35	Pacific Ocean	35°00'S	160°00'E–175°11'E	

Plate 4 presents data from the earlier portion of the deployment from August 18 through August 31, 1996, and is based on DC-8 flight numbers 3–4, and P3-B flight numbers 5–8 and 10 which cover primarily the central part of the Pacific. These flights were selected to provide as compact a longitudinal coverage as possible in conjunction with the ship tracks and surface sites. P3-B flight number 9 was not included in this analysis as it was the only night flight conducted during the mission. Noteworthy, particularly at the northernmost latitudes, are the vertical gradients in the surface data compared with the PBL and free tropospheric levels and the near absence of these differences in the equatorial region. The pronounced low CO_2 mixing ratios observed in the NH can be ascribed to the biosphere's photosynthetic uptake of CO_2 during the northern summer. Within the equatorial zone, CO_2 mixing ratios were relatively constant with altitude as a result of the rapid vertical transport prevalent within the tropics. The surface data
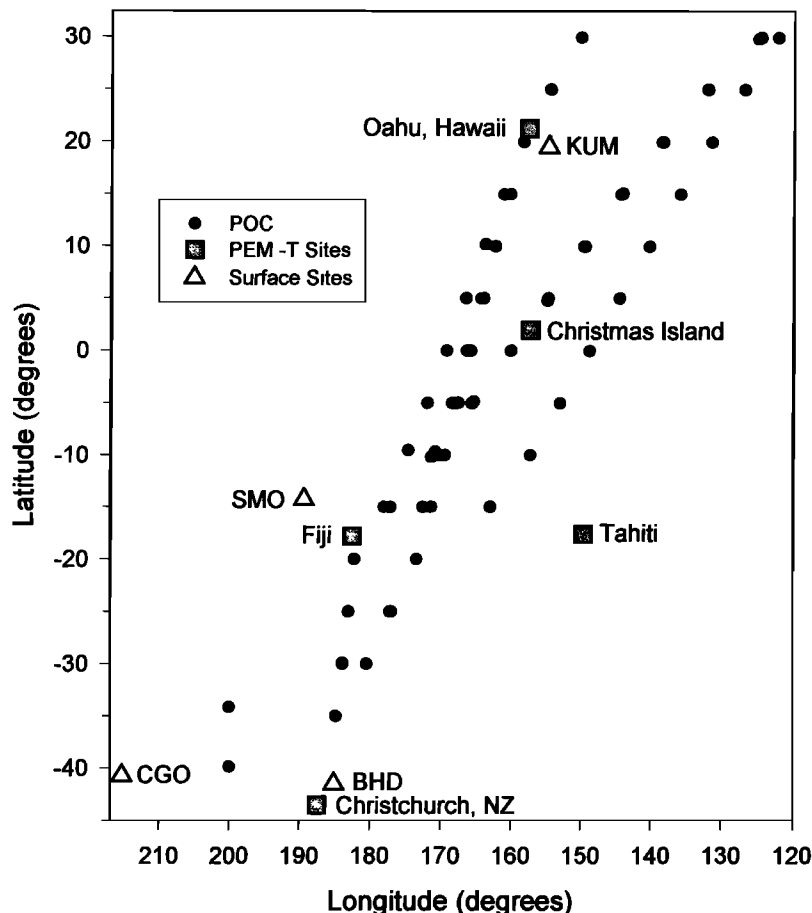
Figure 3. NOAA/CMDL POC ship tracks in conjunction with surface site locations and PEM-T bases of operation.

Table 3. Statistics for Flight Data Depicted in Plate 4

Latitude	Altitude Band, km	Mean, ppmv	(± 1 σ), ppmv	Median, ppmv	N
30°N	1-2	358.87	1.02	359.33	85
	2-6	360.81	0.33	360.68	594
	6-10	360.98	0.45	361.00	640
25°N	1-2	359.94	0.07	359.94	493
	2-6	360.41	0.59	360.67	151
	6-10	361.26	0.12	361.24	1172
20°N	1-2	360.38	0.24	360.40	98
	2-6	360.76	0.45	360.81	2009
	6-10	361.49	0.15	361.51	160
15°N	1-2	360.20	0.40	360.20	217
	2-6	360.69	0.32	360.73	1869
	6-10	360.91	0.34	361.00	1430
10°N	1-2	360.35	0.13	360.37	42
	2-6	360.60	0.49	360.61	1044
	6-10	361.21	0.22	361.28	1194
5°N	1-2	361.49	0.13	361.50	367
	2-6	361.17	0.17	361.14	596
	6-10	361.34	0.20	361.34	972
0°	1-2	361.42	0.24	361.45	1061
	2-6	361.22	0.21	361.25	994
	6-10	361.23	0.13	361.26	142
	10-12	361.46	0.07	361.44	118
5°S	1-2	361.29	0.10	361.28	122
	2-6	361.31	0.20	361.37	485
	6-10	361.27	0.14	361.28	239
	10-12	361.31	0.06	361.32	260
10°S	6-10	361.01	0.18	360.98	406
	10-12	361.39	0.09	361.37	359
15°S	1-2	360.66	0.15	360.65	530
	2-6	361.01	0.22	360.98	312
	6-10	361.07	0.28	361.18	406
20°S	1-2	360.87	0.19	360.95	76

exhibit a peak in the CO_2 concentration from 15°N to 15°S with a maximum value of 361.88 ppmv at the equator. This peak constitutes a CO_2 source attributable to the upwelling of supersaturated CO_2 waters known to occur in the equatorial zone [*Keeling and Heimann*, 1986]. A similar feature is also noted in the PBL and lower troposphere data however, the peak begins at 10°N. Pertinent to these observed increases is the location of the ITCZ at 8°30'N.

Plate 5 illustrates the CO_2 vertical and meridional gradients from the equator to 72°S for the western portion of the basin using data from DC-8 flight numbers 13, 14, and 17 which occurred from September 22 through October 1, 1996. Additionally, statistics for a 5° latitude bin centered over Baring Head New Zealand (BHD) were calculated from a portion of DC-8 flight number 12 for comparison with continuous CO_2 surface measurements conducted by the National Institute of Water and Atmospheric Research Ltd. (NIWA). Of particular interest are the lower CO_2 mixing ratios at the equator compared with those in Plate 4 which were taken almost a month earlier and in the central Pacific. Indeed, a lower concentration is even realized in the surface data. This lower surface value may be ascribed to the fact that the waters of the western Pacific Ocean are not as supersaturated with CO_2 as in the central and eastern portions [*Nakazawa et al.*, 1992] due to the Pacific warm pool or it may be attributable to the influence of NH air. Ten day back trajectories indicate that the air mass encountered at all flight levels originated from the east, or northeast, remaining over water during the entire 10 day period and coming from well within the NH. These lower CO_2 concentrations begin increasing gradually in the lower-altitude bands between the equator and 10°S suggesting convective mixing with the CO_2 rich surface layer.

A major synoptic meteorological feature endemic to the South Pacific Basin is the South Pacific Convergence Zone (SPCZ) which is usually best defined in the January–February time period (H. Fuelburg, personal communication, 1997) and is illustrated in Figure 4. The low southern latitude data shown in Plate 5 was taken when the SPCZ was fairly well defined and characterized by a band of clouds centered near 8°S, with a width of approximately 5° [*Fuelberg et al.*, this issue]. The lack of observed mixing at lower levels between the low NH CO_2 concentrations north of the SPCZ and the higher mixing ratios south of the zone implies that the SPCZ is acting as an effective barrier to meridional transport. Poorer exchange and discontinuities in the CO_2 mixing ratios at the SPCZ have been previously reported by *Heimann and Keeling* [1986], *Tanaka et al.* [1987], and *Nakazawa et al.* [1991]. For an in-depth discussion of the SPZC and ITCZ and their effects on CO_2 and other trace gas distributions during PEM-T, see *Gregory et al.* [this issue].

In Plate 5, the surface and PBL mixing ratios follow one another fairly closely from 5°S to 15°S and then diverge, while exhibiting similar trends, as surface concentrations dip to a minimum at 30°S and once again reflect PBL values at 40°S. Unfortunately, no surface sites currently exist beyond 40°S in the South

Table 4. Statistics for Flight Data Depicted in Plate 5

Latitude	Altitude band (km)	Mean (ppmv)	(±1 σ) (ppmv)	Median (ppmv)	N
0°	1-2	360.68	0.27	360.63	79
	2-6	360.59	0.16	360.62	268
	6-10	360.48	0.10	360.48	95
5°S	1-2	361.48	0.05	361.48	187
	2-6	360.78	0.13	360.79	263
	6-10	360.33	0.19	360.30	485
10°S	6-10	360.66	0.25	360.54	908
15°S	1-2	360.47	0.89	360.88	180
	2-6	361.11	0.28	361.04	288
	6-10	360.81	0.19	360.80	760
20°S	1-2	360.96	0.08	360.96	302
	2-6	361.23	0.19	361.21	199
	6-10	361.25	0.64	361.06	468
	10-12	361.34	0.84	361.01	260
25°S	6-10	361.09	0.12	361.10	427
30°S	1-2	360.16	0.18	360.13	246
	2-6	361.15	0.32	361.08	154
	6-10	360.94	0.06	360.92	39
35°S	1-2	360.74	0.35	360.70	40
	2-6	361.53	0.14	361.53	146
	6-10	361.36	0.16	361.37	510
41°29'S	1-2	360.30	0.17	360.25	295
	2-6	360.35	0.30	360.29	763
	6-10	361.27	0.52	361.37	11
45°S	1-2	360.24	0.14	360.24	39
	2-6	360.91	0.27	361.06	143
	6-10	360.95	0.22	360.94	339
	10-12	360.59	0.04	360.59	56
50°S	6-10	361.03	0.44	360.95	666
	10-12	360.57	0.09	360.56	247
55°S	1-2	360.10	0.06	360.10	42
	2-6	360.18	0.07	360.19	270
	6-10	360.65	0.18	360.71	123
60°S	0-0.5	360.19	0.05	360.19	309
	1-2	360.33	0.08	360.32	223
	6-10	360.38	0.07	360.38	132
65°S	1-2	360.41	0.05	360.41	36
	2-6	360.42	0.05	360.42	507
	6-10	360.42	0.08	360.42	491
70°S	2-6	360.28	0.04	360.27	9
	6-10	360.53	0.08	360.53	148
	10-12	360.62	0.09	360.62	125
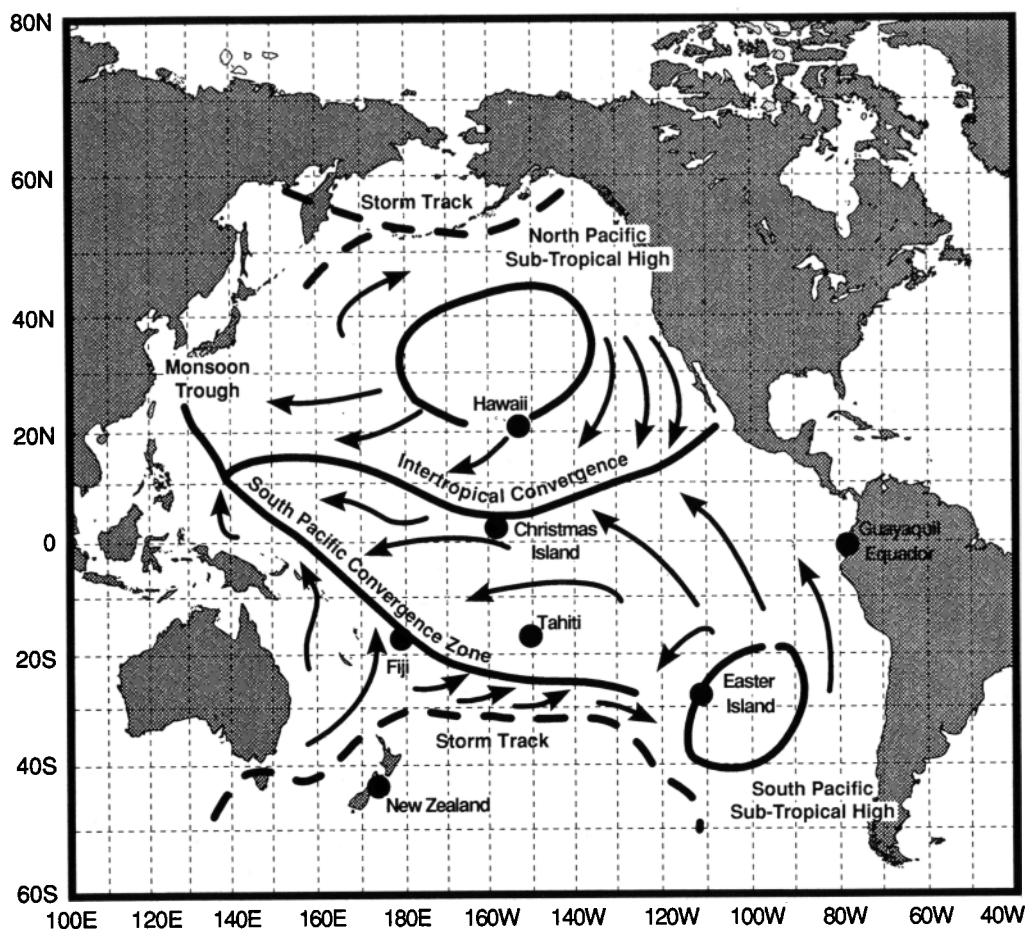
Figure 4. Major features of the atmospheric circulation at the surface over the Pacific Ocean area for June–August [from *Merrill*, 1989].

Pacific Basin for the NOAA/CMDL Network for comparison with the higher latitude flight data. However, if we examine the graph inset in Plate 5, the 1 to 2 km flight data follow a depression-shaped trend from 35°S to 65°S with a CO_2 minimum at 55°S. This overall trend is suggestive of a southern ocean sink operating from south of 15°S. Several authors have mentioned the existence of such a sink but at varying latitudes: 30° to 55°S [*Tans et al.*, 1989], 10° to 45°S (from the Tohoku data set in the work of *Tans et al.* [1989]) and south of 14°S [*Keeling and Heimann*, 1986; *Takahashi et al.*, 1997]. On the basis of model runs using actual $\delta^{13}C$ surface measurements, *Ciais et al.* [1995] describe a Southern Ocean sink from 20°S with the largest portion residing between 30°S and 60°S. They also note recent shipboard measurements of $\delta^{13}C$ in both the atmosphere and water showing a trough at 55°S.

The Southern Oceans are thought to exhibit a marked seasonality in the sources and sinks of CO_2 [*Tans et al.*, 1989]. Some 250,000 ΔpCO_2 measurements assembled by *Takahashi et al.* [1997] exhibit a strong CO_2 sink, with a maximum ΔpCO_2 between the surface water and marine atmosphere in August from 14°S to 50°S. In the austral winter, wind-generated mixing increases the pCO_2 of surface waters in the subpolar and polar Southern Oceans, while photosynthesis decreases it in the summer [*Takahashi et al.*, 1997]. We propose that during PEM-T, a Southern Ocean sink having two distinct zones seasonally out of phase existed: a temperate ocean sink which was at or near its

seasonal maximum between 15°S and 35°S with a trough at 30°S, and a higher-latitude sink from 35°S to 65°S that had recently experienced the winter maximum pCO_2 in the surface waters and was beginning to undergo a decrease in pCO_2 as spring and photosynthesis in the photic zone commenced. The observed rise in CO_2 at the high southern latitudes south of 55° S may be attributable to a source near the Antarctic coast noted by *Tans et al.* [1990].

In the SH, the mid to upper troposphere appears relatively rich in CO_2 compared to the lower troposphere owing to the CO_2 sink at the ocean surface, but also because the vertical distributions of SH CO_2 are controlled by top-down diffusion resulting from the interhemispheric exchange process that occurs more frequently and efficiently at higher altitudes [*Monfray et al.*, 1996; *Anderson et al.*, 1996]. Numerical experiments on tracer particle transport have demonstrated that this process is most pronounced in the NH summer [*Nikaidou*, 1989]. This effect is illustrated at 40°S to 60°S in Plate 5 where CO_2 concentrations in the 6–10 km band exceed those found in the lower troposphere. These levels most likely reflect CO_2 mixing ratios from the previous NH nongrowing season (winter 1995), whereas the lower values in the 10–12 km band can be attributed to the early NH spring (1996). This is further substantiated in viewing Plate 1 where the next wave of NH air is observed propagating southward, being carried further aloft at the ITCZ by deep convection, and then progressing into the midsouthern latitudes at the higher altitudes. At 46°S, this
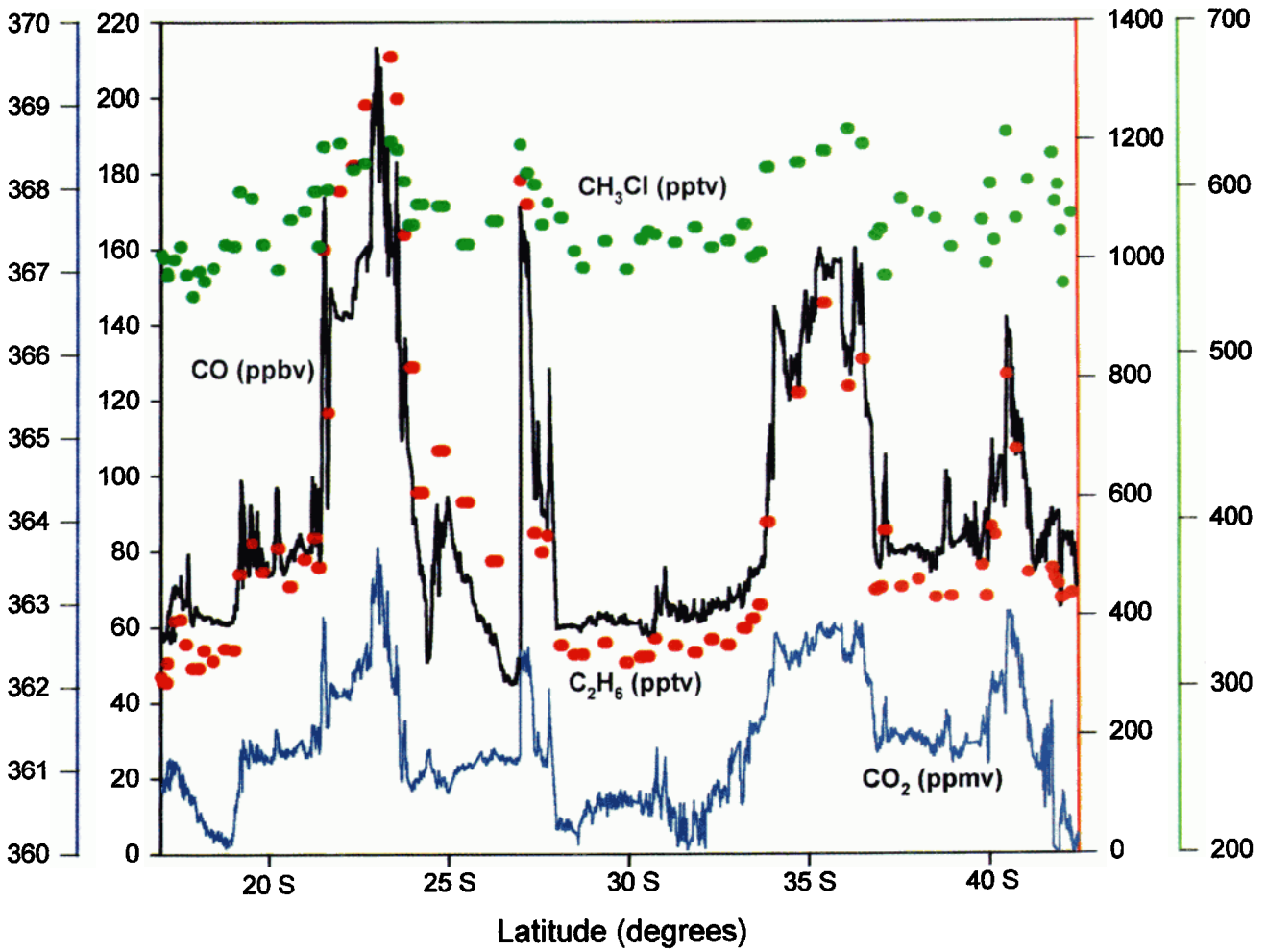
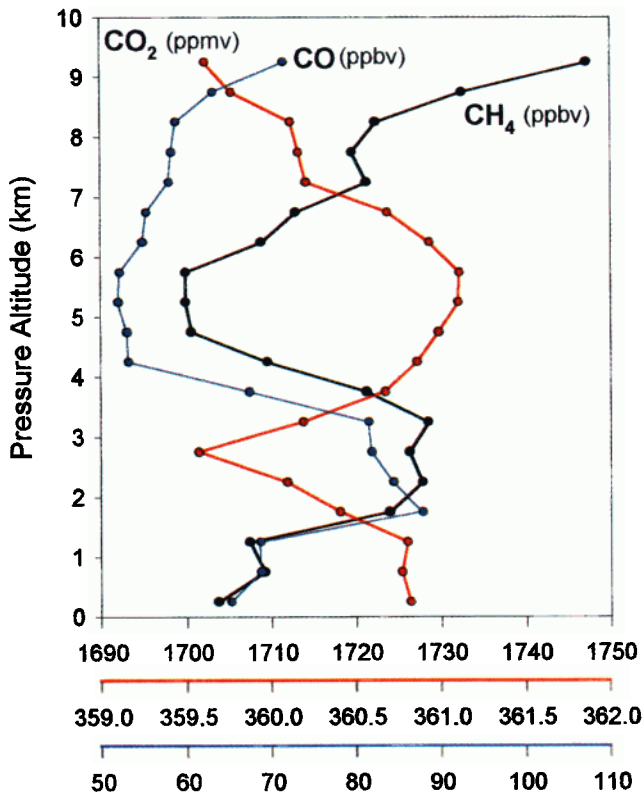**Plate 6.** DC-8 transit from Tahiti to New Zealand September 18, 1996.

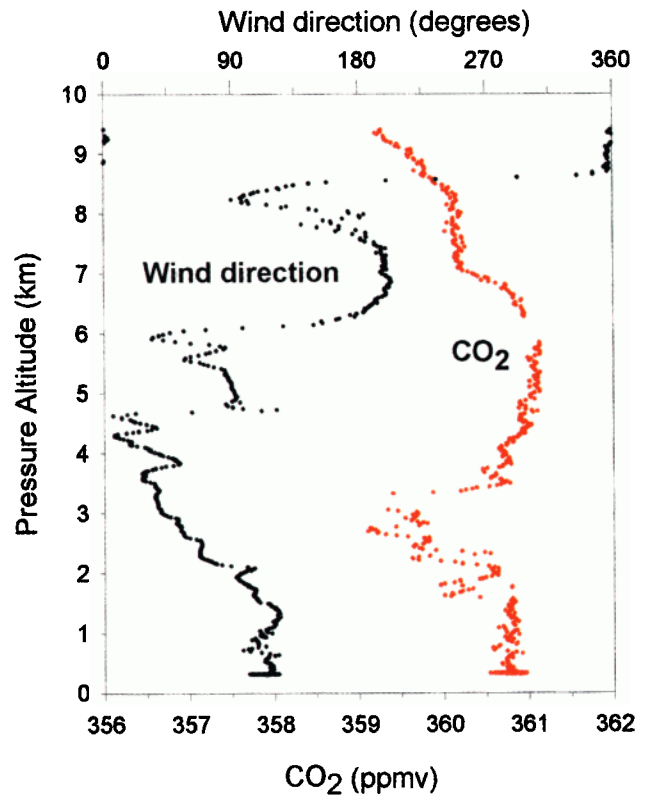**Plate 7.** DC-8 flight north of Easter Island September 10, 1996. Vertical profile at 7°S.

Plate 8. Vertical profile north of Easter Island at 7°S showing low CO$_2$ mixing ratios during periods of north or northeast flow.

NH early spring air is observed both at higher levels and diffusing top-down into lower layers mixing with air from the previous NH winter. Aircraft measurements conducted in the Australian-New Zealand region by *Pearman and Beardsmore* [1984] showed a midtroposphere (3.5 to 5.5 km) concentration maximum in October which lagged behind the upper troposphere (>8.5 km) by a month and attributed this to high altitude meridional transport of NH air into the SH. More recently, however, *Tans et al.* [1989] have proposed that the seasonal cycle at 40°S cannot be entirely ascribed to transport from the NH rather a "tongue" of seasonality exists near the surface from 40°S to 10°S, underneath the mid troposphere, with its seasonality 100°–180° out of phase with higher altitudes. Plate 1 indicates that this may indeed be the case except the tongue appears to extend beyond 40°S. *Tans et al.* [1989] note that this surface layer progressed northward, while the midtropospheric seasonal signal originates from the NH.

In examining Plate 5 at latitudes from 15°S to 40°S, the lower tropospheric CO_2 mixing ratios are observed to exceed those in the mid to upper troposphere. This was due in part to the influence of plumes, most likely from biomass burning, residing within the 2–6 km band encountered during the transit flight from New Zealand to Fiji (J. Logan, personal communication, 1997). We note that at the higher southern latitudes all altitude bands exhibit similar CO_2 concentrations indicating a zone of well mixed air probably owing to recent winter convection.

3.3. Biomass Burning

Although the CO_2 spatial distribution in the South Pacific Basin was significantly influenced by interhemispheric transport, regional processes also played a role in modulating background concentrations. A large number of lower and middle tropospheric pollution events were encountered producing enhanced CO_2 mixing ratios over portions of the remote Pacific. These large scale plumes clearly dominate the western and eastern portions of the basin while the central region remains relatively devoid of these effects as shown in Plate 2. NMHCs, halocarbons, and chlorofluorocarbon emission patterns can be used to characterize these events possibly having anthropogenic sources such as fossil fuel leakage, incomplete combustion, biomass burning, or urban influence [*D. Blake et al.*, 1996]. An air parcel which has been recently augmented by biomass burning would contain elevated levels of CH_4, C_2H_6 (ethane),C_2H_4 (ethene), C_2H_2 (ethyne), additional hydrocarbons, and methyl halides along with CO and CO_2, while exhibiting no urban emitted halocarbons like CFCs or C_2Cl_4 [*N. Blake et al.*, 1996; *D. Blake et al.*, 1996]. Plate 3c illustrates the largest pollution plumes in the western basin were penetrated during the transit flight from Tahiti to New Zealand with the plumes centered at 6.75 km and occurring between 22°S and 41.5°S as shown in Plate 1 by the red color. The accompanying increases in CO_2, CO, CH_4, C_2H_6,C_2H_4, C_2H_2, and CH_3Cl (methyl chloride) with no CFCs or urban tracers such as C_2Cl_4 (perchloroethene) clearly indicate these pollution events were actually large scale biomass burning plumes. Species enhancements of ~3.5 ppmv ΔCO_2, ~155 ppbv ΔCO, and ~1000 pptv ΔC_2H_6 were measured in some cases (Plate 6). Ratios of C_2H_2/CO, which can be used as an approximate indicator of the age of an air mass, were of the order of 1.2 to 1.6 pptv/ppbv implying these plumes were relatively young having somewhat recent inputs [*Smyth et al.*, 1996]. Meteorological analysis determined a westerly flow in the middle to upper tropospheric levels with flight latitudes north of 25°S encountering air originating from western Australia that had later traveled over the northern portion of that continent. Measurements made south of 25°S, were obtained in an air mass originating beyond 60°E that clipped the southern part of Australia as it entered a trough over New Zealand. Observed elevated levels of C_2H_4, having a τ~ 2 days for this latitude and season, along with wind speeds at flight level suggest that the plumes sampled south of 25°S originated in Australia rather than Africa.

The highest CO_2 mixing ratios were observed within biomass burning plumes residing below 5 km off the western South American coast during P3-B flight number 17. Levels of ΔCO_2 within the plumes were ~4 ppmv, whereas ΔCO, ΔC_2H_6, ΔCH_3Cl were markedly higher being ~300 ppbv, ~2000pptv, and ~175 pptv, respectively. A corresponding C_2H_2/CO ratio of ~2 pptv/ppbv for all cases indicates these plumes were less processed and contained fairly recent emissions. Ten-day back trajectories indicate the majority of the flow was from the interior and inland western coast of South America with a minor component originating from interior sections of northern South America. These plumes were therefore attributable to sampling in the biomass burning-influenced continental outflow being advected from the interior of South America out over the Pacific Ocean.

Since biomass burning tends to follow a seasonal pattern, a totally different picture of the basin may be observed in subsequent seasons. During the PEM-T timeframe, however, we find that it plays a significant role in affecting the spatial CO_2 distributions.

3.4. Interhemispheric Transport

Above the Earth's surface, CO_2 in the atmosphere is unreactive and therefore can function as a conservative tracer for elucidating atmospheric mixing processes [*Bolin and Keeling*, 1963]. Plates 1 and 2 are suggestive of NH air depleted in CO_2 propagating southward; however, other tracer species can be used in conjunction with the CO_2 to substantiate the case of NH/SH exchange. DC-8 flight number 8, flown due north out of Easter Island, provides an excellent example of interhemispheric transport occurring in the eastern portion of the South Pacific Basin and the use of CO_2 along with other trace species for verification. A descending vertical profile was performed at the northernmost point of the flight at 7°15′S and is shown in Plate 7 for the trace species CO_2,CO, and CH_4. Above 7 km, CO_2 shows a decreasing trend while CO and CH_4 exhibit elevated levels; evidence of NH air. Accompanying these increases are enhanced levels of C_2H_6, C_3H_8, C_2H_2, CH_3Cl, PAN, fine and ultra fine aerosols, HCFC 141b, HCFC 142b, and HFC 134a. In particular, the HCFC 141b displayed a 1 pptv enhancement corresponding to an air mass "age" of about 6 to 8 months (E. Atlas, personal communication, 1997). The C_2H_2/CO ratio was approximately 0.5 pptv/ppbv indicative of an aged air parcel having no inputs of fresh emissions from combustion sources for at least a week [*Smyth et al.*, 1996]. Noteworthy is a layer with similar chemical signatures occurring between 1.5 and 4 km. As shown in Plate 8, within the layers of low CO_2 values the wind is due north or northeast, while elevated levels are measured when winds are from the south or southeast. Meteorological analysis shows southeast flow skirting along and off the coastal area of west-central South America, whereas the southern flow is from the western Pacific Ocean. During periods of low CO_2 mixing ratios, a northern hemispheric flow was clearly indicated that emanated from Central America.

3.5. Upwelling

A survey of data collected from 1958 to 1962 revealed a natural release of CO$_2$ at the ocean surface in the tropical oceanic areas [*Bolin and Keeling*, 1963]. Subsequent surface measurements of $^{13}C/^{12}C$ ratios have demonstrated that the source can be attributed to the release of CO$_2$ from seawater [*Keeling and Carter*, 1984] along the equator where the north and south equatorial currents from each hemisphere meet causing a divergence or upwelling. Indications are the observed atmospheric peak is a stationary source (except possibly during El Niño events) resulting from waters supersaturated in CO$_2$. Several authors have since noted this equatorial source at varying degrees of latitude and source strengths, for example, 12°N to 12°S, 1.3 GtC [*Heimann and Keeling*, 1989], 15°N to 15°S, 1.3 GtC [*Tans et al.*, 1990], 10°N to 10°S, 0.9 ± 1.3 GtC [*Ciais et al.*, 1995], and 14°N to 14°S, 0.46 to 1.04 GtC [*Takahashi et al.*, 1997]. Plate 1 indicates an equatorial CO$_2$ source occurring approximately between 8°N and 8.5°S with a zone of intensity from 6.5°N to 1°S. Interestingly, these elevated CO$_2$ concentrations at the lower altitudes appear confined to a vertical column that is bounded on either side by the ITCZ and SPCZ suggesting that the enriched CO$_2$ column may actually shift in time with the seasonal movement of these zones. However, since CO$_2$ sources/sinks can only be inferred from these data, low CO$_2$ air traveling above the surface in the absence of strong surface fluxes must also be considered as a plausible explanation for this equatorial "source." Plate 1 also demonstrates the importance of vertical trace gas profiles, particularly in potential source/sink regions, as they provide an additional constraint for global scale trace gas budgeting models [*Fung et al.*, 1991].

Upwelling from the depths of cold, mineral-rich, supersaturated CO$_2$ water also occurs on the eastern sides of oceans. South America has one of the most vigorous areas of upwelling in the world off its western coastline due to the southeasterly trade winds enabling the northward flowing Humboldt, or Peru, current to reach the surface. Enhancements in CO$_2$ mixing ratios of the order of 1.4 ppmv were observed during P3-B low-altitude flight legs (~0.1 km) off the South American coast as shown in Plate 3a. Accompanying these elevated CO$_2$ concentrations were notable levels of DMS which is produced by the metabolic processes in certain types of algae residing in the nutrient-rich waters therefore suggestive of an upwelling source. Other tracers such as CO and CH$_4$ demonstrated no departure from background levels during these low-altitude runs having concentrations of ~60 and ~1700 ppbv, respectively. Evidence of the upwelling signature in the free troposphere was dwarfed by the outflow from the continent's interior of biomass burning plumes containing high CO$_2$ mixing ratios.

3.6. Summary and Conclusions

High-precision CO$_2$ measurements were made over a significant portion of the South Pacific Basin from August 18 to October 5, 1996, as part of the PEM-T mission. These tropospheric measurements represent the most extensive aerial CO$_2$ data set in this region therefore greatly augmenting the existing database. Results from this rich data set offer insight into the source/sink processes occurring within this remote region. We find that interhemispheric transport plays a key role in determining the spatial distribution of CO$_2$ in the SH particularly at the upper levels. However, near the surface, from south of 10°S, there exists a "tongue" of air seasonally out of phase with the midtropospheric levels that cannot be attributed to transport from

the NH. Biomass burning activities, producing elevated levels of CO$_2$, contributed significantly to the zonal inhomogenity observed around the basin perimeter. A CO$_2$ source was observed in the equatorial region, whereas a Southern Ocean sink beginning at 15°S was inferred from these data. These results will likely have significant implications for the development and testing of atmospheric global carbon cycle models. PEM-T occurred in the months preceding an El Niño which is currently described as "the climatic event of the century." A follow-on mission is tentatively scheduled for the austral fall of 1999 during the anticipated waning months of this event.

References

Anderson, B. E., G. L. Gregory, J. E. Collins Jr., G. W. Sachse, T. J. Conway, and G. P. Whiting, Airborne observations of spatial and temporal variability of tropospheric carbon dioxide, *J. Geophys. Res.*, *101*(D1), 1985–1997, 1996.

Blake, D. R., T. -Y. Chen, T. W. Smith Jr., C. J. L. Wang, O. W. Wingenter, N. J. Blake, F. S. Rowland, and E. W. Mayer, Three-dimensional distribution of nonmethane hydrocarbons and halocarbons over the northwestern Pacific during the 1991 Pacific Exploratory Mission (PEM-West A), *J. Geophys. Res.*, *101*(D1), 1763–1778, 1996.

Blake, N. J., D. R. Blake, B. C. Sive, T.-Y. Chen, F. S. Rowland, J. E. Collins Jr., G. W. Sachse, and B. E. Anderson, Biomass burning emissions and vertical distribution of atmospheric methyl halides and other reduced carbon gases in the South Atlantic region, *J. Geophys. Res.*, *101*(D19), 24151–24164, 1996.

Bolin, B., and C. D. Keeling, Large-scale atmospheric mixing as deduced from the seasonal and meridional variations of carbon dioxide, *J. Geophys. Res.*, *68*(D13), 3899–3920, 1963.

Callendar, G. S., On the amount of carbon dioxide in the atmosphere, *Tellus*, 10, 243–248, 1958.

Ciais, P., P. P. Tans, J. W. C. White, M. Trolier, R. J. Francey, J. A. Berry, D. R. Randall, P. J. Sellers, J. G. Collatz, and D. S. Schimel, Partitioning of ocean and land uptake of CO$_2$ as inferred by $\delta^{13}C$ measurements from the NOAA Climate Monitoring and Diagnostics Laboratory Global Air Sampling Network, *J. Geophys. Res.*, 100(D3), 5051–5070, 1995.

Conway, T. J., P. Tans, L. S. Waterman, K. W. Thoning, K. A. Masarie, and R. H. Gammon, Atmospheric carbon dioxide measurements in the remote global troposphere, 1981–1984, *Tellus, Ser. B*, *40*, 81–115, 1988.

Conway, T. J., and L. P. Steele, Carbon dioxide and methane in the Arctic atmosphere, *J. Atmos. Chem.*, *9*, 81–89, 1989.

Conway, T. J., P. P. Tans, L. S. Waterman, K. W. Thoning, D. R. Kitzis, K. A. Masarie, and N. Zhang, Evidence for interannual variability of the carbon cycle from the National Oceanic and Atmospheric Administration/Climate Monitoring and Diagnostics Laboratory Global Air Sampling Network, *J. Geophys. Res.*, *99*(D11), 22831–22855, 1994.

Fuelberg, H. E., R. E. Newell, S. P. Longmore, Y. Zhu, D. J. Westberg, E. V. Browell, D. R. Blake, G. R. Gregory, and G. W. Sachse, A meteorological overview of the PEM-Tropics period, *J. Geophys. Res.*, this issue.

Fung, I., J. John, J. Lerner, E. Matthews, M. Prather, L. P. Steele, and P. J. Fraser, Three-dimensional model synthesis of the global methane cycle, *J. Geophys. Res.*, *96*, 13033–13065, 1991.

Gregory, G. L., et al., Chemical characteristics of Pacific tropospheric air in the region of the ITCZ and SPCZ, *J. Geophys. Res.*, this issue.

Heimann, M., and C. D. Keeling, Meridional eddy diffusion model of the transport of atmospheric carbon dioxide, 1, Seasonal carbon cycle over

the tropical Pacific Ocean, *J. Geophys. Res., 91*(D7), 7765–7781, 1986.

Heimann, M., and C. D. Keeling, A three-dimensional model of atmospheric CO₂ transport based on observed winds, 2, Model description and simulated tracer experiments, in *Aspects of Climate Variability in the Pacific and Western Americas, Geophys. Monogr. Ser.*, vol. 55, pp. 237–275, edited by D. H. Peterson, AGU, Washington, D. C., 1989.

Hoell, J. M., D. D. Davis, D. Jacob, M. Rodgers, R. E. Newell, H. Fuelberg, R. J. McNeal, J. Raper, and R. J. Bendura, The Pacific Exploratory Mission in the tropical Pacific: PEM-Tropics A, August–September 1996, *J. Geophys. Res.*, this issue.

Intergovernmental Panel on Climate Change, *Climate Change: The IPCC Scientific Assessment*, edited by J. T. Houghton, G. J. Jenkins, and J. J. Ephraums, 365 pp., Cambridge Univ. Press, New York, 1990.

Intergovernmental Panel on Climate Change, *Climate Change 1992: The Supplementary Report to the IPCC Scientific Assessment*, edited by J. T. Houghton, B. A. Callander, and S. K. Varney, 200 pp., Cambridge Univ. Press, New York, 1992.

Jaffe, B., in *New World of Chemistry*, p. 358, Silver Burdett, New York, 1942.

Keeling, C. D., and A. F. Carter, Seasonal, latitudinal, and secular variations in the abundance and isotopic ratios of atmospheric CO₂, 2, Results from oceanographic cruises in the tropical Pacific Ocean, *J. Geophys. Res., 89*(D3), 4615–4628, 1984.

Keeling, C. D., and M. Heimann, Meridional eddy diffusion model of the transport of atmospheric carbon dioxide, 2, Mean annual carbon cycle, *J. Geophy Res., 91*(D7), 7782–7796, 1986.

Keeling, C. D., T. P. Whorf, M. Wahlen, and J. van der Plicht, Interannual extremes in the rate of rise of atmospheric carbon dioxide since 1980, *Nature, 375*, 666–670, 1995.

Kirchhoff, V.W.J.H., J. R. Alves, F. R. da Silva, and J. Fishman, Observations of ozone concentrations in the Brazilian Cerrado during the TRACE A field expedition, *J. Geophys. Res., 101*(D19), 24029–24042, 1996.

Komhyr, W. D., L. S. Waterman, and W. R. Taylor, Semiautomatic nondispersive infrared analyzer apparatus for CO₂ air sample analyses, *J. Geophys. Res., 88*, 1315–1322, 1983.

Marland, G., and T. A. Boden, CO₂ emissions-modern record, in *Trends 1991: A Compendium f Data on Global Change*, edited by T. A. Boden, R. J. Sepanski, and F. W. Stoss, 665 pp., Carbon Dioxide Inf. Anal. Cent., Oak Ridge Nat. Lab., Oak Ridge, Tenn., 1991.

Marland, G., R. J. Andres, and T. A. Boden, Global, regional, and national CO₂ emission estimates from fossil fuel burning, cement production, and gas flaring: 1950–1994, *NDP-030/R7*, Carbon Dioxide Inf. Anal. Cent. (CDIAC) Oak Ridge, Tenn., spring 1997.

Matsueda, H., and H. Inoue, Measurements of atmospheric CO₂ and CH₄ using a commercial airliner from 1993 to 1994, *Atmos. Environ., 30*(10/11), 1647–1655, 1996.

Merrill, J. T., Atmospheric long range transport to Pacific Ocean, pp. 15–50 in *Chemical Oceanography*, vol. 10, edited by J. P. Reiley and R. Duce, Academic Press, San Diego, Calif., 1989a.

Monfray, P., M. Ramonet, and D. Beardsmore, Longitudinal and vertical CO₂ gradients over the subtropical/subantarctic oceanic sink, *Tellus, Ser. B, 48*, 445–456, 1996.

Nakazawa, T., K. Miyashita, S. Aoki, and M. Tanaka, Temporal and spatial variations of upper tropospheric and lower stratospheric carbon dioxide, *Tellus, Ser. B, 43*, 106–111, 1991.

Nakazawa, T., S. Murayama, K. Miyashita, S. Aoki, and M. Tanaka, Longitudinally different variations of lower tropospheric carbon dioxide concentrations over the North Pacific Ocean, *Tellus, Ser. B, 44*, 161–172, 1992.

Nikaidou, Y., Three-month tracer diffusion experiments and their seasonal difference in interhemispheric mass exchange in the troposphere, in *Research Activities in Atmospheric and Oceans Modelling, Rep. 13, WMO/TD, 332*, pp. 7.21–7.22, World Meteorol. Org., Geneva, 1989.

Pearman, G. I., and D. J. Beardsmore, Atmospheric carbon dioxide measurements in the Australian region: Ten years of aircraft data, *Tellus, Ser. B, 36*, 1–24, 1984.

Sachse, G. W., R. C. Harriss, J. Fishman, G. F. Hill, and D. R. Cahoon, Carbon monoxide over the Amazon basin during the 1985 dry season, *J. Geophys. Res., 93*, 1422–1430, 1988.

Santer, B. D., et al., A search for human influences on the thermal structure of the atmosphere, *Nature, 382*, 39–46, 1996.

Smyth, S. B., et al., Factors influencing the upper free tropospheric distribution of reactive nitrogen over the South Atlantic during the TRACE A experiment, *J. Geophys. Res., 101*(D19), 24165–24186, 1996.

Takahashi, T., R. A. Feely, R. F. Weiss, R. H. Wanninkhof, D. W. Chipman, S. C. Sutherland, and T. T. Takahashi, Global air-sea flux of CO₂: An estimate based on measurements of sea-air pCO₂ difference, *Proc. Natl. Acad. Sci. U. S. A., 94*, 8292–8299, 1997.

Tanaka, M., T. Nakazawa, and S. Aoki, Seasonal and meridional variations of atmospheric carbon dioxide in the lower troposphere of the northern and southern hemispheres, *Tellus, Ser. B, 39*, 29–41, 1987.

Tans, P. P., T. J. Conway, and T. Nakazawa, Latitudinal distribution of the sources and sinks of atmospheric carbon dioxide derived from surface observations and an atmospheric transport model, *J. Geophys. Res., 94*(D4), 5151–5172, 1989.

Tans, P. P., I. Y. Fung, and T. Takahashi, Observational constraints on the global atmospheric CO₂ budget, *Science, 247*, 1431–1438, 1990.

Thoning, K. W., P. P. Tans, and W. D. Komhyr, Atmospheric carbon dioxide at Mauna Loa Observatory, 2, Analysis of the NOAA GMCC data, 1974–1985, *J. Geophy. Res., 94*, 8549–8565, 1989.

B. E. Anderson and S. A. Vay, Atmospheric Sciences Division, NASA Langley Research Center, Hampton, VA 23681-0001. (e-mail: s.a.vay@larc.nasa.gov)

D. R. Blake, Department of Chemistry, University of California, Irvine, CA 92717.

J. E. Collins Jr., Science and Technology Corporation, 101 Research Drive, Hampton, VA 23666.

G. W. Sachse, Aerospace Electronic Systems Division, NASA Langley Research Center, Hampton, VA 23681-0001.

D. J. Westberg, Science Applications International Corporation, 1 Enterprise Parkway, Suite 300, Hampton, VA 23666.